Mapping Variability of Soil Water Content and Flux across 1-1,000 m scales using the Actively Heated Fiber Optic Method

Chadi Sayde[1], Javier Benitez Buelga[2], Leonor Rodriguez-Sinobas[2], Laureine El Khoury[1], Marshall English[1], Nick van de Giesen[3], and John S. Selker[1]

[1]Dept. of Biological & Ecological Engineering, Oregon State University, Corvallis, OR, USA

[2] Dept. of Rural Engineering, Technical University of Madrid, Madrid, Spain

[3]Water Management Civil Engineering and Geosciences, Delft University of Technology, Delft, Netherlands

First revision of manuscript submitted to

Water Resources Research

American Geophysical Union

1. Abstract

The Actively Heated Fiber Optic (AHFO) method is shown to be capable of measuring soil water content several times per hour at 0.25 m spacing along cables of multiple kilometers in length. AHFO is based on distributed temperature sensing (DTS) observation of the heating and cooling of a buried fiber optic cable resulting from an electrical impulse of energy delivered from the steel cable jacket. The results presented were collected from 750 m of cable buried in three 240 m co-located transects at 30, 60, and 90 cm depths in an agricultural field under center pivot irrigation. The calibration curve relating soil water content to the thermal response of the soil to a heat pulse of 10 W m^{-1} for 1 minute duration was developed in the lab. This calibration was found applicable to the 30 and 60 cm depths cables, while the 90 cm depth cable illustrated the challenges presented by soil heterogeneity for this technique. This method was used to map with high resolution the variability of soil water content and fluxes induced by the non-uniformity of water application at the surface.

2. Introduction

Soil moisture is highly variable in time and space, and is the most important factor in controlling the spatio-temporal variability of surface water and energy balances [*Western et al.*, 2003; 2004]. Quantification of these dynamic spatial patterns have been difficult to obtain, holding back the understanding of soil moisture dynamics and interacting hydrological processes [e.g., *Western et al.*, 2001, 2003; *Wilson et al.*, 2004].

Processes such as infiltration [*Flury et al.*, 1994; *Raats*, 2001] and plant-water dynamics [*Porporato et al*., 2004] are fundamentally controlled by soil water content at the point scale. Such processes are of a particular importance in agricultural systems management. Detailed information on soil moisture is needed for applications including improved yield forecasting and irrigation scheduling [*Shmugge*, 1980].

Sayde et al. [2010] provided a laboratory demonstration of the feasibility of the Actively Heated Fiber Optics (AHFO) method for distributed, 0.25-10,000 m scale measurement of soil moisture content. This approach is based on observing the heating and cooling of a buried fiber optic cable through the course of a pulse application of energy as monitored by a distributed temperature sensing (DTS) system.

The ability of DTS to report the temperature each meter along fiber optic cables in excess of 10,000 m in length at high temporal frequency has opened many important opportunities in environmental monitoring [e.g., *Selker et al*., 2006a; 2006b; *Tyler et* *al.*, 2009], including the estimation of the surface water content and evapotranspiration under suitable conditions from computing the energy balance of the soil using temperature measurements at several depths [*Steele-Dunne et al*., 2010].

The use of actively heated fiber optics for observation of subsurface water movement has been mentioned previously [e.g., *Weiss*, 2003; *Perzlmaier et al*., 2004; *Aufleger et al*., 2005; and *Perzlmaier et al*., 2006; *Streig and Loheide*, 2012] and our team demonstrated the feasibility of using AHFO for accurate distributed measurement of soil water content [*Sayde et al*., 2010]. Most recently The AHFO method has been used to monitor water wetting bulbs formation around drip emitters in a laboratory experiment [Gil-Rodriguez et al., 2012] and water distribution inside a lysimeter [Ciocca et al., 2012]. In these applications the fiber optic is encased in a stainless steel capillary tube surrounded by copper windings or a molded aluminum encasement, all of which are enclosed in an electrical insulation sufficient for the voltage employed and appropriate for direct burial. The metallic component of the fiber optic cable is used as an electric resistance heater to inject heat concentric to the fiber optic sensing element into the surrounding soil, while the optical fiber is used as a thermal sensor to monitor the resulting temperature changes. The soil thermal properties are a function of soil texture, bulk density, temperature, and soil moisture content. Under ambient temperature conditions, soil moisture content can be inferred by analysis of thermal responses of specific soils to the heat pulse. *Sayde et al.* [2010] presented a novel approach to the interpretation of these heat pulse signals which was optimized for use with DTS. Here, the thermal response of the soil is calculated in the form of an integral of the temperature increase over time in the presence of energy input, which represents the product of change in temperature and lapsed time (T_{cum}) from the start of the heat pulse. Soil moisture content is computed via T_{cum} through a calibration equation. The theory is that higher water content will reduce the change in temperature relative to drier soil, reducing this integral. This procedure yielded relatively accurate estimation of soil moisture content. *Sayde et al.* [2010] found that the absolute accuracy of the soil water content measurements varied approximately linearly with water content. At volumetric moisture content of 0.05 $m^3\ m^{-3}$ the standard deviation of the readings was <0.01 $m^3\ m^{-3}$, and at 0.41 $m^3\ m^{-3}$ volumetric moisture content the standard deviation was 0.046 $m^3\ m^{-3}$. *Sayde et al.* [2010] indicated that this error could be further reduced by increasing the signal-to-noise ratio which could be accomplished by: averaging several heat-pulse results; using a more precise DTS unit; increasing the heating intensity; or increasing the duration of the heating. In a small scale field test of the AHFO method, *Streig and Loheide* [2012] reported a RMSE of 0.016 $m^3\ m^{-3}$ for soil moisture content $\leq$ 0.31 $m^3\ m^{-3}$, and a RMSE of 0.05 $m^3\ m^{-3}$ for higher soil moisture content values. The results of both experiments were obtained using DTS with approximately ten fold lower precision that those currently available, suggesting that more precise soil moisture measurements are now feasible, although calibration of the method to specific soils will be required to realize this potential.

The objective of this work is to evaluate the performance and the applicability of this technology under field conditions. In this work, we test the ability of the AHFO method to capture small scale (<1 m) variation in soil water content and fluxes as imposed by controlled spatially variable water application at the soil surface. We will also discuss methods to improve the calibration procedure and the quality of the AHFO outputs.

3. Materials and Methods

3.1 Site description

The study site is located on a farm near Echo, OR. The 26 ha agricultural field was irrigated by a center pivot system designed to deliver water up to 4 cm d^{-1}. The spacing between consecutive emitters decreased with distance from the center while their discharge rates increased, as required to ensure a spatially even application depth (Appendix 1).

The field was planted with corn on March 17th, 2009 and harvested on September 15th, 2009. The soil is sandy loam and the average bulk density, determined from 26 non-disturbed soil samples at four locations from soil surface to 90 cm depth, was 1.67 g cm^{-3} with a standard deviation of 0.12 g cm^{-3}.

3.2 Field installation and data collection procedure

In October 2007, three Fiber Optic (FO) cables were installed below the tillage depth along a 240 m transect (Figure 1) at 30, 60, and 90 cm below the surface. A plow system was designed and built for this installation. The plow was made of a 2.54 cm thick steel blade with trailing-edge tubes through which the cables were introduced underneath the soil surface (Figure 2). By ganging the three tubes along the trailing edge of the plow, we installed three sets of cables at the three depths in a single pass. The most rapid possible re-establishment of native soil conditions surrounding the installed cables was critical to our considerations; therefore, the plow blade was held at a 45 degree angle from vertical, so that the weight of the soil would assist in closing the cut made in the soil. The first and the last 8 m ends of each of the three FO cables sets were submerged in an ice bath for calibration and validation of the DTS readings. The FO cable (BruSteel® manufactured by Brugg Cable, Brugg, Switzerland) deployed in the field had an outer diameter (OD) of 3.8×10^{-3} m and is composed of four optical fibers encased in a central stainless steel capillary tube (OD 1.3×10^{-3} m; inner diameter ID 1.07×10^{-3} m) surrounded by 12 stainless steel strands (OD 4.2×10^{-4} m stainless steel wires), all of which were enclosed in a 7.3×10^{-4} m thick nylon jacket. The metallic components of the cable had an electrical resistance of $0.365\ \Omega\ m^{-1}$ at 20 ºC.

By splicing the end of an optical fiber at one depth to the end of an optical fiber at the following depth, The FO cables were optically connected between the three depths to form a continuous optical light-path allowing simultaneous temperature reading along the whole installation. A DTS unit (SensorTran DTS 5100 M4, Houston, TX), connected to the FO system, recorded temperature every 0.5 m along the fiber-optic cable, with a spatial resolution of 1 m for each single measurement. The average temperature reading frequency was 0.2 Hz.

The high voltage power supply available at the center pivot system provided an average of 490 VAC to heat one of the three sections with an average power intensity of 11 W m^{-1}. A series of timers and relays insured that each of the three cable section was heated separately for 1 minute duration every hour. A voltmeter located at the center pivot, was employed to measure the applied voltage.

Spatial variability in soil water content and flux was imposed by varying the water application pattern at the soil surface. The center pivot was programmed to repeatedly pass back and forth covering a 21^{o} angle sector of the center pivot circle such that only the 3 outer sections of the cable transect (described below) were covered by the center pivot path, while the section nearest the pivot was not irrigated. The center pivot operation and the discharging emitters' location and spray geometry were modified to apply four distinct but simultaneous water application treatments along the FO cables transect location as follows:

- Section 1: From 0 to 55 m radial position. No water was applied over or immediately adjacent to section 1.

- Section 2: From 55 to 110 m radial position. The emitters were shrouded in open plastic sleeves such that water was applied directly below the emitters instead of the typical circular pattern (Figure 2 of the supplementary material). This insured a high application rate directly below the emitters while the inter emitters locations were kept dry. The last sprinkler in section 2 (sprinkler # 19) was turned off to insure separation of treatment with section 3. After 20 minutes from the irrigation start time, the plastic sleeve of sprinkler # 13 burst and this sprinkler was turned off for the remaining of the experiment.
- Section 3: Radially from 110 to 158 m. Of the 12 emitters covering this section, the inner-most was turned off (to create separation of treatments); the next discharged at its regular position; while the next ten were grouped into five sets of paired emitters (Figure 3 of the supplementary material).
- Section 4: From 158 to 240 m. Alternating application. Of the 21 emitters covering this section, 10 were turned off and the remaining emitters were applying water at their regular positions, either as isolated individual emitters, or in pairs of emitters. (see Table 1 and Figure 4 of the supplementary material).

Water was applied for 7 h. Heat pulses were applied every hour for 48 h starting 6 h prior to water application.

3.3 Data interpretation

The heat pulse signals were interpreted using the methodology described in *Sayde et al.* [2010] wherein the thermal response of the soil is calculated as an integral temperature change relative to the pre-heated temperature due to energy input over time:

$$T_{cum} = \int_{0}^{t_0} \Delta T \, dt \qquad \text{Eq. 1}$$

Where T_{cum} (°C s) is the integral of ΔT (°C), the DTS reported temperature change from the pre-pulse temperature due to energy input during the total time of integration t_0(s). The soil moisture content is inferred from T_{cum} through a calibration equation which under laboratory conditions yielded +\- 1.5 % errors in estimation of soil moisture content [*Sayde et al.*, 2010].

3.4 Lab calibration

The soil specific calibration of the equation relating the thermal response (T_{cum}) to soil water content θ was obtained from a laboratory experiment. This was carried out using the same field fiber optic cable but installed in a cylindrical plastic barrel of 0.51 m diameter and 0.91 m height of repacked soil from the experimental site prepared to reproduce the average bulk density observed in the field. An outlet was installed 0.1 m above the bottom and a 0.012 m diameter perforated hose was fitted to the inside of the drainage port and wound in a tight spiral which covered the bottom of barrel to provide an easily controlled lower boundary condition.

Within the column, 10 m of BruSteel® FO cable in a helicoidal geometry was supported by three vertical steel rods 6.4 x 10^{-3} m in diameter.The cable made eight 0.3 m diameter helical coils, spaced 0.1 m vertically, starting 0.05 m from the bottom and ending at the surface of the soil (0.9 m from the bottom). The soil was collected from the soil surface to the 70 cm depth at two locations near the fiber optic cable in the field. The soil was air-dried before being added to the column in 20 kg lifts. After each lift, the soil was compacted to the volume that corresponds to the prescribed soil bulk density. No settling was observed during the experiment.

From the 17 m continuous section of the FO cable, a 4-m unheated section was placed in a temperature monitored water bath for calibration and validation purposes. The next 11.4 m of cable (including the section in the soil column) was heated by connecting the stainless steel windings to variable voltage AC current source (Staco® Variable Autotransformer Type 3PN1010). The ~ 0.1% drop in voltage along the 12 AWG copper connecting wires was negligible in our calculations. A digital timer with a precision of ± 0.01 % (THOMAS® TRACEABLE® Countdown Controller 97373E70) controlled the duration of heat pulses.

The calibration data were obtained in three phases: Phase I) θ ranging from 0.23 to 0.15 m^3 m^{-3}; Phase II) θ ranging from 0.11 to 0.05 m^3 m^{-3}; and Phase III) θ at saturation (0.40 m^3 m^{-3}). The conditions for phase I were established by saturating the soil column from its bottom. Then, this column was gravity drained for 3 days with its top covered to reduce evaporation. At this point, DTS measurements of 6 s resolution were taken during 1 minute, 10 W m^{-1} heat pulses. Three replicates with the same combinations of power intensity and pulse duration were applied. Following the final DTS measurements in the drained column, 14 volumetric samples were collected at seven depths from the soil surface downwards to 10 cm from the column bottom.

In phase II, the top cover of the column was removed, and the column was left exposed to the ambient room environment for three months to generate a smooth transition from air-dry soil at the column top to nearly saturated conditions at the column base. After DTS measurements, 32 soil samples were gathered for water content determination. These were collected following 12.5 cm spans along the cable moving from the soil surface up to 50 cm from the bottom.

In phase III, the remaining 50 cm of the soil column that had not yet been excavated was saturated from the bottom up.

Two DTS instruments were used during the lab calibration:

- SensorTran DTS 5100 M4 in phase I: This DTS unit recorded temperature every 0.5 m along the fiber-optic cable, with a spatial resolution of 1 m for each single measurement. The average reading frequency was 0.17 Hz. The manufacturer reported temperature resolution at 2.5 km, 1 m spatial resolution, and 0.17 Hz is 0.53 °C.

- Silixa Ultima (Silixa, London, England) in phase II and III: This DTS unit recorded temperature every 0.125 m along the fiber-optic cable, with a spatial resolution of 0.29 m. The average reading frequency was 1 Hz. The manufacturer reported temperature resolution at 2.5 km, 0.29 m spatial resolution, and 1 Hz is 0.3 °C, which is consistent with the results we observed for our much shorter cable.

3.5 Thermal properties of the soil column

Measurement of soil thermal properties were made to allow comparisons of the calibration equations obtained from the lab experiments to the ones from either analytical or numerical solutions of the heat transport models. Thermal conductivity and specific heat were measured with an accuracy of 5% using a dual-needle probe (Decagon KD2-Pro® equipped with SH-1® dual-needle) in nine undisturbed soil samples and for soil water contents ranging from saturation (0.40 m^3 m^{-3}) to air-dry conditions. The nine samples were randomly chosen from the set of 14 non-disturbed soil samples used for the determination of soil water content distribution across the soil column in phase I of the lab calibration. For the air-dry conditions, the previously oven dried samples were kept exposed to ambient air for a period of two months before thermal properties were measured. For the saturated conditions, the same set of samples was submerged in water for 24 hours period prior to measurements. For soil water content between saturation and air-dry conditions, the saturated samples were placed in a pressure chamber for three days to reach equilibrium at each of the four pressure levels (0.07, 0.33, 0.66, and 1.0 bar), after which soil water content was determined gravimetrically and soil thermal properties measured as described above. Subsequently, the samples were exposed to ambient air conditions for 48 h and then covered for another 48 h before the soil water content was determined gravimetrically and the soil thermal properties were measured. Finally, all the samples were oven dried to 105 ^{o}C and left covered for 12 h in ambient room temperature to cool down prior to the measurement of thermal properties.

3.6 Adjusting for the variation in the applied power intensity

In the field deployment, the actual applied power may vary between heat pulses due to: 1) ± 2 V fluctuation in the applied voltage, and 2) thermal dependency of the electrical conductivity of the FO cable’s heating element (the stainless steel component). For a constant resistance power is proportional to the square of applied voltage, thus the fluctuation on the nominal 480 V supply contributed to a 0.9% uncertainty in the applied energy. Changes in the electrical resistance of the FO heating element were a function of the cable temperature. Thus, it could be accurately estimated via the DTS measured cable temperature.

Since the soil thermal heat flow and heat storage processes in this system are linear, the temperature increase, and in consequence value of T_{cum}, are proportional to the power applied, as seen in both the cylindrical source transient and the line source transient methods [see *Blackwell*, 1954; *de Vries and Peck*, 1958; *Jaeger*, 1965; *Shiozawa and Campbell*, 1990; *Bristow et al.*, 1994]. Thus the effects of temporal variation in the power can be eliminated by linearly scaling observed temperatures to those that would have been obtained at a common reference power intensity.

3.7 Calculating water front travel time

To compare the soil water content response for the different wetting regimes in the field, a time-lagged cross-correlation analysis was performed between the time series of soil moisture change at each particular position along the FO cable installed at 30 cm depth and those of its corresponding position along the FO cable at the 60 cm depth. The cross-correlation method has been employed successfully to study time-lag relationship between soil moisture content at variable depths [*Georgakakos et al.*, 1995; *Mahmood and Hubbard*, 2007; *Mahmood et al.*, 2012].

The Matlab function "Xcorr" was used to calculate the cross-correlation coefficient, $\hat{R}_{xy}(m)$, associated with each time lag (m) tested as follows:

$$\widehat{R}_{xy}(m) = \begin{cases} \sum_{n=0}^{N-m-1} x_{n+m}\, y_n & m \geq 0 \\ \widehat{R}_{yx(-m)} & m < 0 \end{cases} \qquad \text{Eq. 2}$$

Here x and y are soil water content at the 30 and the 60 cm depth, normalized by their initial value (m = 0). *N* is the length of the *x* and *y* vectors.

The maximum correlation coefficients value is used to identify the appropriate time lag to represent the wetting-front travel time at each location (see Table 2 in the supplementary material for a list of maximum correlation coefficient per location and its corresponding time lag value).

3.8 Calculating Water Fluxes

For each particular location (*i*) along the fiber optic cables and for each particular depth (*d*) a wetting front velocity (V_{id}) and a flux (F_{id}) can be calculated as follows:

$$V_{id} = D_{id}\, l_{id}^{-1} \qquad \text{Eq. 3}$$

and

$$F_{id} = V_{id}\, \Delta\theta max_{id} \qquad \text{Eq. 4}$$

Where:

- D_{id} is the distance between two successive depths, D_{id} = 30 cm in our case,
- l_{id} is the time period elapsed between the wetting front arrival at two successive depths (h),
- $\Delta\theta max_{id}$ is the maximum change in volumetric water content ($m^3\, m^{-3}$).

3.9 Assessing the impact of the convective heat transfer from moving water

The calibration equation to translate T_{cum} measurements into soil water contents was developed in the labortory under hydrostatic conditions. One concern is the validity of this calibration curve under convective heat transfer conditions from moving water i.e. when water infiltrates at a velocity that is significant in comparison to the velocity of the heating front. A common practice to assess if the convective heat transfer from moving fluid can be omitted from the heat transfer calculation is to evaluate the Peclet number (*Pe*). *Pe* compares the relative strength of convective to diffusive transport of the same physical quantity, applicable to heat and mass transport processes. The critical value of *Pe* depends upon the application. It is common to employ the criteria of Pe <1 to delineate transport processes dominated by diffusion (e.g., ONDRAF/NIRAS, 2002 as cited in *Huysmans and Dassargues*, 2004). However, this is not universal, for instance *de Marsily* (1986) took mass transport processes to be controlled by diffusion for $Pe < 2$. *Wilson et al.* (1993) took the transition between diffusion controlled and advection controlled mass transport to occur $1.5 < Pe < 15$ (as cited in *Huysmans and Dassargues,* 2004). We will take the most conservative value since we seek to identify where the laboratory diffusion-only results are applicable to the field, and assume that diffusion dominates for $Pe < 1$.

For heat transfer in porous media, *Pe* can be calculated as (*Bear*, 1972; *Hopmans et al.*, 2002):

$$Pe = V_{conv} L/\kappa \qquad \text{Eq. 5}$$

with

$$V_{conv} = v\,\theta\,C_w/C_{bulk} \qquad \text{Eq. 6}$$

Where V_{conv} is the convective heat pulse velocity in a porous media (m s^{-1}) i.e. the heat flow by the moving liquid phase, v is the average pore water velocity (m s^{-1}), θ is the soil volumetric water content (m^3 m^{-3}), C_w is the water volumetric heat capacity (J m^{-3} K^{-1}), C_{bulk} the soil volumetric heat capacity (J m^{-3} K^{-1}), and L is the characteristic length (m). For a heat pulse probe application, *Hopmans et al.* [2002] defined L as being the characteristics length of the porous media approximated by the medium grain size. We will follow a more conservative approach here and define L as the effective distance traveled by the convective water front during the heating time t (t= 60 s in our case) such as:

$$L = v\,t\,\theta \qquad \text{Eq. 7}$$

Substituting V_{conv} by (2) and L by (3) in (1) we get:

$$Pe = (v\,\theta)^2 t\,C_w/(C_{bulk}\kappa) \qquad \text{Eq. 8}$$

4. Results

4.1 Lab calibration results and system performance

A calibration equation was fitted to the data relating measured soil water content to measured T_{cum} (Figure 3). The gravimetric samples from the soil column had an average bulk density (ρ_b) of 1.63 g cm^{-3} with a standard deviation (σ_b) of 0.06 g cm^{-3}, in the range of values found in the field (ρ_b=1.67 g cm^{-3} and σ_b=0.12 g cm^{-3}) and those published for this soil by the Natural Resources Conservation Service NRCS (1.15-1.70 g cm^{-3} range; Table 1).

T_{cum} became insensitive to variation in soil water content at high water content ($S >$ 0.4; Figure 3). The shape of the calibration curve for very dry soil conditions (e.g., $S <$ 0.1) also suggests that T_{cum} is insensitive to variation in soil water content in this range. In the later case, this can be explained by observing the behavior of the soil thermal conductivity (λ) at low soil water content. In fact, λ has been shown to be nearly constant from water contents ranging from zero to a critical value (θ_{cr}) (Figure 4a). This could be explained by the water geometry transitions from pendular to funicular [*de Vries*, 1963; *Tarnawski and Leong*, 2000]. The value of θ_{cr} tends to be dependent on the clay content of the soil [*Tarnawski and Leong*, 2000; *McInnes*, 1981]. The observed θ_{cr} value (0.03 m^{3}m^{-3}) is in agreement with *de Vries'* [1963] recommendation of using θ_{cr} values of 0.03 m^3 m^{-3} for coarse soils. This behavior is also observed in the thermal diffusivity curve (Figure 4b).

For soil water content ranging from 0.04 to 0.40 $m^3 m^{-3}$ ($0.1 < S < 1$) the slope in the relationship relating θ to T_{cum} decreases with soil water content (Figure 3) indicating that error in soil water content estimation is expected to increase with increasing soil water content as observed in *Sayde et al.* [2010] and *Gil-Rodriguez et al.* [2012].

The error in T_{cum} , σ_{Tcum}, was determined by measuring the variability in T_{cum} over repeated measurements at constant soil moisture content, as in *Sayde et al.* [2010]. Under the lab conditions, with a Silixa Ultima-S, 85% of the variability in σ_{Tcum} (3.18 °C s) was due to instrument noise when 1s and 0.12 m sampling resolutions were employed. The remaining 15% is believed to have been caused by voltage fluctuation during heating and spatial variability of soil thermal properties in the soil column. However, the noise in T_{cum} obtained with the SensorTran 5100 unit was 12.6 °Cs for the 6 s and 0.5 m sampling resolutions conditions, a level at which any other source of error was undetectable. The maximum error in soil water content determination was observed at saturation (Figure 5). This error was 0.03 $m^3 m^{-3}$ and 0.11 $m^3 m^{-3}$ for the Silixa Ultima-S and the SensorTran 5100, respectively.

4.2 Field test results

4.2.1 Soil water content

The calibration equation developed in section 2 (Figure 3), was used to translate T_{cum} values observed over the three depths cables in the field to soil water content. The slope of the calibration curve is high for near saturated soil and low at low soil water content. As pointed out by *Sayde et al*. [2010] this implies the method is less sensitive in wet conditions. Furthermore, if for any reason the values of T_{cum} are biased low, then it is possible to compute values that are not in the range of the calibration results, and therefore yield undefined soil moisture. On the other hand, if the calibration curve is biased high, then the soil moisture estimates from T_{cum} will not include high water contents.

The 90 cm depth soil water contents, as estimated using the calibration curve of Figure 3, clearly showed the characteristics of a high- bias. Though the changes in T_{cum} at the 90 cm depth were of same magnitude and with similar spatial patterns as those observed at the 30 and the 60 cm depths (Figure 6), these did not result in significant soil water content changes as were observed with the 30 and the 60 cm depths. The calibration challenges are discussed with further details in section 5.

The 30 and the 60 cm DTS estimated soil water content corresponded to those expected from the four patterns of spatial variability imposed at the soil surface. Section 1 (between 0 and 55 m) was not irrigated, and as expected, no significant water change was detected at either depth (Figure 7 and 8). Between 55 and 110 m (Section 2), the nine constraining sleeves imposed high-rate (0.35 l s^{-1}) water application directly below each emitter, as seen at the nine locations with high soil water content change in this section (Figure 7 and 8). The average total water applied over the nine wetted locations was 72 mm. In section 3 (between 110 m and 158 m), the four wide strips of high soil water content change observed at both 30 and 60 cm depths (Figure 7 and 8) correspond to the expected patterning of the paired emitters.

In section 4 (from 158 m to the end), at the 30 cm depth the highest soil water content increases were observed at the locations of the operating emitters (Figure 8a). For the 60 cm depth cable, the pattern was the same but the variation in soil water content was more modest than under the other treatments (Figure 8b), as expected due to the lower water application. The average total water applied over section 4 was 32 mm while this value was 72 mm and 54 mm over the wetted locations of section 2 and section 3 respectively.

4.2.2 Soil Water flux density

To calculate the water front travel time from depth 30 cm to depth 60 cm, the data obtained along the fiber optic cable were separated into two groups based on the maximum change in soil water content observed at the 30 cm depth locations. The first group of data represents data retrieved from locations where $\Delta\theta > 0.05$ m^3 m^{-3} at the 30 cm depth, with the second group being the remaining locations (see Figure 9a).

For the first group, the average time lags were 0.64 h (standard deviation of 0.97 h), 2.55 h (standard deviation of 1.21 h), and 3.46 h (standard deviation of 2.91 h) for sections 2, 3, and 4, respectively. This variation follows the pattern of water application at the soil surface for the three treatment sections: section 2 received the highest application rate for all locations in group 1, and section 4 the lowest application rate.

The same method was used to calculate the wetting front travel time from depth 60 cm to depth 90 cm. Since the T_{cum} to moisture content calibration developed for the upper soil was observed unsuitable for the 90 cm depth, the time series of change in T_{cum} (from pre-irrigation conditions) for both 60 and 90 cm depths are employed instead of the time series of change in soil water content. As before, the calculated time lag was separated into two groups; Group 1 includes the time lag for location where $\Delta\theta$ at 60 cm was > 0.05 $m^3 m^{-3}$, and Group 2 for where $\Delta\theta$ at 60 cm was < 0.05 $m^3 m^{-3}$ (Figure 9b). For the Group 1, the average time lags were 0.93 h (standard deviation of 1.72 h), 3.33 h (standard deviation of 1.49 h), and 5.89 h (standard deviation of 1.83 h) for sections 2, 3, and 4, respectively. On average, the wetting front movement was 32% faster between the 30 and the 60 cm depths than between the 60 and the 90 cm depths.

Readers should be aware of the high uncertainty associated with the use of the time lag to estimates the wetting front traveling time for section 2 of the fiber optic cable location. In section 2, about half of the time lag values calculated for the different positions at the 30 cm depth and for a lesser extent at the 60 cm depth have either negative or zero values. This is a clear indication that the transit times were not long enough to be accurately quantified based on 1-h measurement intervals between moisture content measurements at the highest fluxes. Thus, the results of section 2 were considered non-reliable to estimate the water front traveling time and will not be used in the further analysis.

The estimates of the wetting front traveling times in sections 3 and 4 allow calculation of the wetting front velocity and associated flux.

As expected, larger water fluxes were computed below the locations that showed higher increase in water content (Figure 10, and Table 2), which in turn are associated with the locations of the discharging emitters as discussed in a previous section. The fluxes diminish with depth following the pattern of water application. Average flux was reduced by 41% over section 3, and 71% over section 4 (see Table 2). This was expected in section 3 compared to section 4, as the applied discharge rate was the highest, and localized over a smaller wetted area.

To assess if the convective heat transfer from moving water in the soil was large enough to bias T_{cum}-θ calibration, an average *Pe* was calculated for each section. For section 3, the average time lag observed over the locations with $\Delta\theta > 0.05$ m^3 m^{-3} was 2.55 hr between the 30cm and 60cm depths and 3.3 hr between the 60cm and 90cm depths (an average time lag of 2.9 hr over all depths). For section 4, the average time lag observed over the locations with $\Delta\theta > 0.05$ m^3 m^{-3} was 3.64 hr between the 30 cm and 60 cm depths and 5.89 hr between the 60 cm and 90 cm depths (an average time lag of 4.8 hr over all depths). This yields an average water front velocity of 0.029 mm s^{-1} for section 3 and 0.017 mm s^{-1} for section 4. For each of these velocities, Equation 8 was used to calculate *Pe*. The values for *k* were obtained from the laboratory measurements described in section *3.5* (see Figure 4b). Equation 8 yielded *Pe*= 0.013

for section 3, and *Pe*= 0.0048 for section 4. Even for section 2 where the water front velocity was considered overestimated and unreliable *Pe*= 0.18. These results indicate that the effect of the flowing water convective heat transfer on the T_{cum} based estimated θ can be considered negligible for the conditions of these experiments.

5. Discussion

The calibration relating DTS measured T_{cum} to soil water content (Figure 3) was determined in a rather laborious laboratory experiment. The soil column was only representative of the top 70 cm of the soil, the maximum depth in the field from which soil was collected. In keeping with unpublished observations of a textural transition observed during the installation of neutron probe tubes, beyond 70 cm depth the soil had different thermal properties and thus the calibration equation obtained in laboratory experiment was not directly applicable to the 90 cm depth cable. These results illustrate that a more practical calibration methodology will be needed for the method to find broad adoption, and ideally this would be an in situ approach given the complexity of typical soils.

Another disadvantage of the calibration conducted in laboratory that even if the soil was collected in situ and repacked to original bulk density, it has been disturbed during this process. In this case, the grain to grain contact might be different which can also affect the water bridges formations. The soil restructuring can lead to deviation in the measured thermal properties of the soil. That said, this experiment was conducted in an agricultural field that was subject to periodic plowing up to 90 cm depth. The effect of this plowing process and the post plowing soil recovery on homogenizing the plowed profile and reshuffling the grain to grain contact is expected to be of similar magnitude of preparing the soil column in the laboratory.

The most direct, although time intensive, calibration method is to simultaneously measure T_{cum} and soil moisture content over the full range of soil moisture conditions at as many locations as there are differing soil conditions and then use the water content and T_{cum} values as in Figure 3. Alternatively one could measure thermal conductivity, diffusivity and water content over the full range of soil moisture conditions either in the field or in undisturbed soil samples (similar to figure 4) at as many locations as there are differing soil conditions. One could then use heat transport numerical simulation models to generate calibration curve relating T_{cum} to soil water content for that particular cable and soil. In either case, measuring thermal properties of soil and soil water content over the full range of soil water content at all location presents a daunting challenge.

Practical insights can be gained from looking at the relationship between thermal conductivity (λ) and soil water content (θ). Most models relating λ to θ assume that the fundamental shape is universal, and simply scaled for each soil [*Johansen* 1975; *Campbell* 1985; *Cote and Konrad* 2005; *Lu et al.* 2006]. The scaling parameters are generally obtained by optimizing the model fit to λ and θ measurements. For the model described by *Campbell* [1985] one only needs a value for measurements of bulk density and two measurements of λ for wet and dry conditions.

In principle, calibration curves relating T_{cum} to soil water content would be expected to share the same basic shape; steep slope toward high water content and flat toward low soil water content, as observed in this work, in *Sayde et al.* [2010], and in *Gil-Rodriguez et al.*, [2012]. This suggests that calibration curves for different soil types could be scaled from few reference curves using measurements from the field representing end members of water content. The only fundamental difference in shape that we might expect between curves of different soil types is the θ_{cr} value below which T_{cum} is held nearly constant (see section 4.1).

Another factor that will significantly impact the measurements' quality using the AHFO method is the DTS instrument performance. The two instruments employed in this study resulted in a 3.5 times difference in the determination of soil moisture error (Figure 5) for the same heat pulse characteristics and soil water conditions. The large difference in measurements' quality is due to the instruments temperature measurement error. This error was computed for the instruments' finest spatial resolution, which differed between the instruments (see section 3.4 for more details). Note that the DTS reported temperature is calculated from the ratio of the magnitudes of anti-Stokes to Stokes scattered light, which are a function of total number of reflected photons. By the law of large numbers, the number of observed photons follows a normal distribution with a standard deviation decreasing by the square root of the total number of photons observed [*Selker et al.*, 2006a]. Since the number of photons observed is a 1:1 function of the fiber volume from which photons are scattered, the noise level is inversely proportional to the square root of the measurement spatial length (see Selker et al., 2006 for more details). If the spatial resolution for both DTS instruments used in this work is set equal, the error in soil moisture determination would have decreased by an additional factor of two when employing the higher performance Silixa Ultima-S DTS.

Other factors may also impact the quality of the DTS measurements such as the temporal drift of the soil temperature due to the diurnal temperature cycle or water fluxes propagation through the soil. One way to evaluate the impact of the temporal variability of the soil temperature is to look at the soil temperature temporal trend during a 5 min period directly before the start of the heat pulse. For each heat pulse, the average slope for the linear regression of temperature vs. time for this 5 min period has been calculated for each of the four sections. The highest deviation from zero slope was -0.44 10^{-3} °C s^{-1}. It was observed at 1 hour before the start of irrigation in section 4. Over a heating period of 60 s, this slope value might have caused a drop of 0.0264 °C in the soil temperature which is equivalent to less than 5% of the instrument noise i.e. in this experiment the effect of the soil temperature temporal variability is negligible when compared to overall instrument error.

6. Conclusions

AHFO method is capable of capturing a complex spatial pattern of soil water content, reporting from many hundreds of points simultaneously. These data, for instance, allowed estimation of local soil water flux. delineation of these patterns with point-measurement instruments would not be feasible. Larger scale measurements techniques, such as Cosmic-Ray probes [*Zreda et al., 2008*] and remote sensing, might be able to provide an average picture of the change in soil water content, but, do not capture the 1-1000 m scale processes observed in this experiment which are of importance in irrigated agriculture, and natural systems (e.g. preferential flows and contaminant transport).

The results showed that soil moisture contents and fluxes can be measured and monitored at a range of values (ranging from dry to saturated conditions) that is significantly larger than the <0.06 range m^3 m^{-3} reported by *Weiss* [2003] and more informative than the qualitative “dry, wet or saturated” assessment reported by *Perzlmaier et al.* [2004; 2006]. This improvement is mainly due to the use of a data interpretation method (i.e. *The time integral of temperature deviation* developed by *Sayde et al.* [2010]) that is appropriate to the DTS method wherein precision of temperature reporting is a direct function of the interval of photon integration.

AHFO applications allow operator control over the heat signal that is injected into the soil. At the expense of added power and complexity, this provides certain advantages over the diurnal cycle driven heat signal employed by the passive distributed temperature sensing method for soil moisture estimation described by *Steele-Dunne et al*. [2010]. Specifically, it may be applied at any depth and any time whereas the passive heat signal attenuates with depth so that it is generally only applicable <30 cm depth under conditions of significant diurnal heat flux (e.g. not under dense vegetative canopy, or on cloudy or winter days).

Error in soil water content estimates due to instrumentation was reduced considerably (from 0.11 to 0.03 $m^3 m^{-3}$ at saturation) when a DTS with better performance was employed in the laboratory experiment. A generally applicable Peclet Number approach showed that water content estimates were shown to be independent of soil-water flux for the conditions employed here.

The calibration of the AHFO method remains challenging. Though yet to be developed, in principle, a calibration procedure could take advantage of the expected similarity between the relationships between T_{cum} and θ to that of thermal conductivity and θ.

7. Acknowledgements

The authors gratefully thank Kent Madison and Madison farm for their tremendous support during the installation and operation of the Fiber Optic system at their farm.

The authors also thank Richard Cuenca, and Scott Tyler for their helpful conversations about this experiment, and Maria Gil Rodriguez for helping in preparation of the matlab scripts. We gratefully acknowledge the support of the National Science Foundation (grant 1129003), NASA (grant NASA 10-THP-0054) and the Oregon Experiment Station for their critical financial support. We appreciate the editor, associate editor, and three anonymous reviewers' dedication to understanding the contents of this work, resulting in comments and questions that greatly improved the final manuscript.

8. References

Aufleger, M., M. Conrad, S. Perzlmaier, and P. Porras (2005), Improving a Fiber Optics tool for monitoring leakage, *Hydro Review Worldwide*, 13(4):18-23.

Blackwell, J.H. (1954), A transient-flow method for determination of thermal constants of insulating materials in bulk, *J. Appl. Phys.*, Vol. 25, pp. 137–144.

Blöschl, G., and M. Sivapalan, (1995), Scale issues in hydrological modeling: a review, *Hydrological Processes* 9:251-290.

Bristow, K.L., R.D. White, and G.J. Kluitenberg (1994), Comparison of single and dual probes for measuring soil thermal properties with transient heating, *Australian Journal of Soil Research*, 32:447-464.

Campbell, G.S. (1985), Soil Physics with BASIC, Elsevier: New York.

Cote, J., and J.M. Konrad (2005), Thermal conductivity of base-course materials, *Canadian Geotechnical Journal*, 42:61-78.

Farouki, O.T. (1986), Thermal properties of soils. Series on rock and soil mechanics, Vol. 11, *Trans Tech Publications*, Clausthal-Zeller- feld, Germany.

Flury, M., H. Flüler,W.A. Jury, and J. Leuenberger (1994), Susceptibility of soils to preferential flow of water: a field study, *Water Resour. Res*. 30, 1945–1954.

Georgakakos, K. P., D.-H. Bae, and D.R. Cayan (1995), Hydroclimatology of continental watersheds: 1. Temporal analyses, *Water Resour. Res*., 31(3), 655-675.

Hausner, M.B., F. Suárez, K. E. Glander, N. van de Giesen, J.S. Selker and S.W. Tyler (2011), Calibrating Single-Ended Fiber-Optic Raman Spectra Distributed Temperature Sensing Data, *Sensors*, DOI:10.3390/s111110859.

Jaeger, J.C. (1965), Application of the theory of heat conduction to geothermal measurements, In 'Terrestrial Heat Flow.' (Ed. W. H. K. Lee.) *American Geophysical Union Monograph,* Vol. 8, pp. 7-23.

Johansen, O. (1975), Thermal conductivity of soils, Ph.D. thesis, University of Trondheim, Trondheim, Norway, US Army Corps of Engineers, Cold Regions Research and Engineering Laboratory, Hanover, N.H. CRREL, Draft English Translation 637.

Lu, H., C.J. Moran, and I.P. Prosser (2006), Modeling sediment delivery ratio over the Murray Darling Basin, *Environmental Modeling and Software* 21:1297–308.

Mahmood. R., and K.G. Hubbard (2007), Relationship between soil moisture of near surface and multiple depths of the root zone under heterogeneous land uses and varying hydroclimatic conditions, *Hydrological Processes,* 21(25):3449-3462.

Mahmood R., A. Littell, K.G. Hubbard , and J. You (2012), Observed data-based assessment of relationships among soil moisture at various depths, precipitation, and temperature, *Applied Geography* 34:255-264.

McInnes, K.J. (1981), Thermal conductivities of soils from dryland wheat regions of Eastern Washington, MS Thesis, Washington State Univ., Pullman, WA.

Perzlmaier, S., M. Aufleger, and M. Conrad (2004), Distributed fiber optic temperature measurements in hydraulic engineering. - Prospects of the heat-up method, In: Proceedings of the 72nd ICOLD Annual Meeting - Workshop on Dam Safety Problems and Solutions-Sharing Experience, Seoul, South Korea, May 16-22, 2004, Korean National Committee on Large Dams (KNCOLD), Seoul, p.31.

Perzlmaier, S., K.-H. Straßer, Th. Strobl, and M. Aufleger (2006), Integral seepage monitoring on open channel embankment dams by the DFOT heat pulse method, Proceedings of the 22nd Congress of the International Commission on Large Dams, Barcelona, Spain. Q. 86 – R. 12, p 145-164.

Porporato, A., E. Daly, and I. Rodríguez-Iturbe (2004), Soil water balance and ecosystem response to climate change, *American Naturalist*, 164 (5):625–633.

Raats, P.A.C. (2001), Developments in soil–water physics since the mid 1960s, *Geoderma*, 100:355–387.

Sayde. C., C. Gregory, M. Gil-Rodriguez, N. Tufillaro, S. Tyler, N. van de Giesen, M. English, R. Cuenca, and J.S. Selker (2010), Feasibility of soil moisture monitoring with heated fiber optics, *Water Resources Research*, 46, W06201, doi:10.1029/2009WR007846.

Shiozawa, S., and G.S. Campbell (1990), Soil thermal conductivity, *Remote Sens. Rev.*, 5:301–310.

Selker, J.S., L. Thévenaz, H. Huwald, A. Mallet, W. Luxemburg, N. van de Giesen, M. Stejskal, J. Zeman, M. Westhoff, and M.B. Parlange (2006a), Distributed Fiber Optic Temperature Sensing for Hydrologic Systems, *Wat. Resour. Res.*, 42, W12202, doi:10.1029/2006WR005326.

Selker, J.S., N. van de Giesen, M. Westhoff, W. Luxemburg, and M.B. Parlange (2006b), Fiber optics opens window on stream dynamics, *Geophysical Research Letters*, 33, L24401, doi:10.1029/2006GL027979.

Schmugge, T.J. (1980), Effect of texture on microwave emission from soils, *IEEE Trans. Geosci. Remote Sens.*, GE-18:353-361.

Steel-Dunne, S.C., M.M. Rutten, D.M. Krzeminska, M. Hausner, S.W. Tyler, J.S. Selker, T.A. Bogaard, and N.C. van de Giesen (2010), Feasibility of soil moisture estimation using passive distributed temperature sensing, *Water Resour. Res.*, 46, W03534, doi:10.1029/2009WR008272.

Strieg, A.M., and S.P Loheide II (2012), Heated distributed temperature sensing for field scale soil moisture monitoring, *Ground Water*, *50 (3):340-347.*

Tarnawski V.R., and W.H. Leong (2000), Thermal conductivity of soils at very low moisture content and moderate temperatures, *Transport in Porous Media*, 41(2):137-147.

Tyler, S.W., J.S. Selker, M.B. Hausner, C.E. Hatch, T. Torgersen, C.E. Thodal, and G. Schladow (2009), Environmental temperature sensing using raman spectra DTS fiber-optic methods, *Wat. Resour. Res*., doi:10.1029/2008WR007052.

van de Giesen, N., S. Steele-Dunne, J. Jansen, O. Hoes, M.B. Hausner, S.W. Tyler, and J.S. Selker (2012), Double-Ended Calibration of Fiber-Optic Raman Spectra Distributed Temperature Sensing Data. *Sensors*, 12(5), 5471-5485, doi:10.3390/s120505471.

de Vries, D.A., and A.J. Peck (1958), On the cylindrical probe method of measuring thermal conductivity with special reference to soils. Part 1. Extension of theory and discussion of probe characteristics, *Aust. J. Phys.*, 11: 255-71.

de Vries, D.A. (1963), Thermal properties of soils. *Physics of Plant Environment*. Ed. W.R. Van Wijk., 210-35. North-Holland: Amsterdam.

Weiss, J.D. (2003), Using fiber optics to detect moisture intrusion into a landfill cap consisting of a vegetative soil barrier, *J. Air & Waste Manage. Assoc.*, 53:1130-1148.

Western A.W., G. Blöschl G, and R.B. Grayson (2001), Towards capturing hydrologically significant connectivity in spatial patterns, *Water Resour. Res.* 37:83–97.

Western, A.W., R.B. Grayson, and G. Blöschl (2002), Scaling of soil moisture: A hydrologic perspective, *Annu. Rev. Earth Planet. Sc.*, *30*:149-180.

Western, A.W., S. Zhou, R.B. Grayson, T.A. McMahon, G. Blöschl, and D.J. Wilson (2004), Spatial correlation of soil moisture in small catchments and its relationship to dominant spatial hydrological processes, *Journal of Hydrology,* 286:113–134.

Wilson, J.D., A.W. Western, and R.B. Grayson (2004), Identifying and quantifying sources of variability in temporal and spatial soil moisture observations, *Water Resources Research* 40, W02507.

Zreda, M., D. Desilets, T.P.A. Ferré, and R.L. Scott (2008), Measuring soil moisture content non-invasively at intermediate spatial scale using cosmic-ray neutrons, *Geophys. Res. Lett.*, 35, L21402.

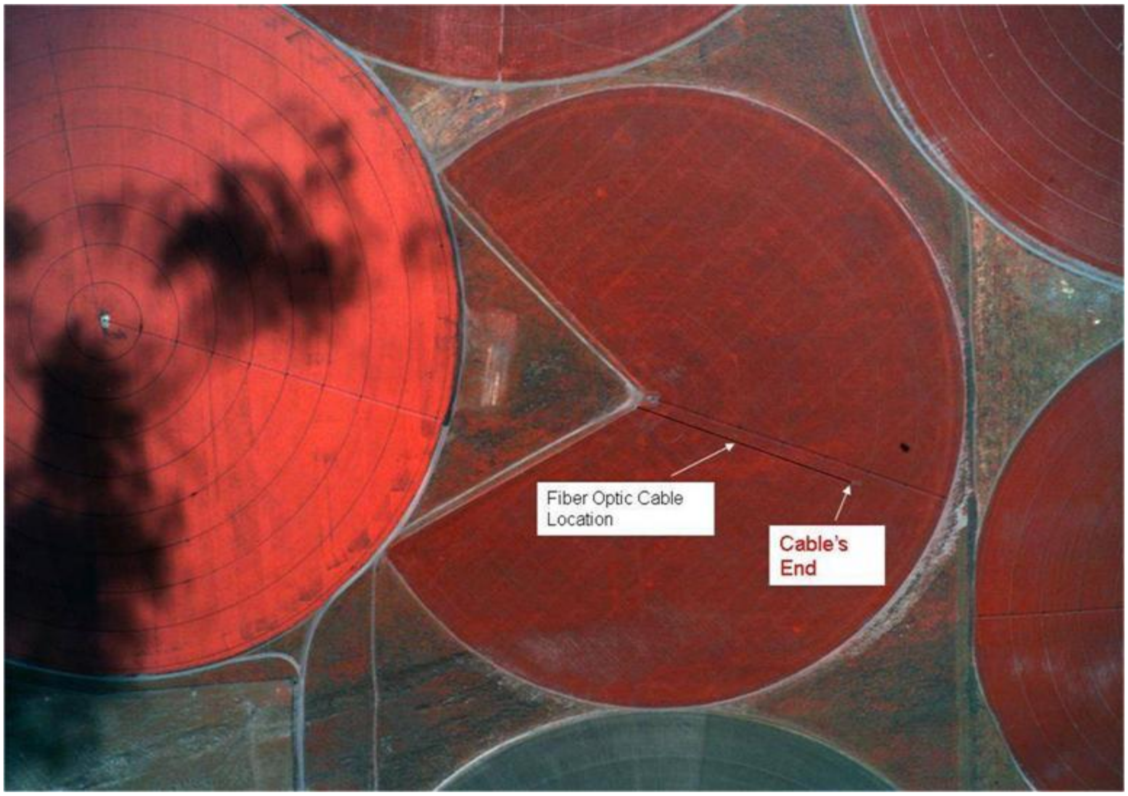

Figure 1 Fiber Optic transect location in the field.

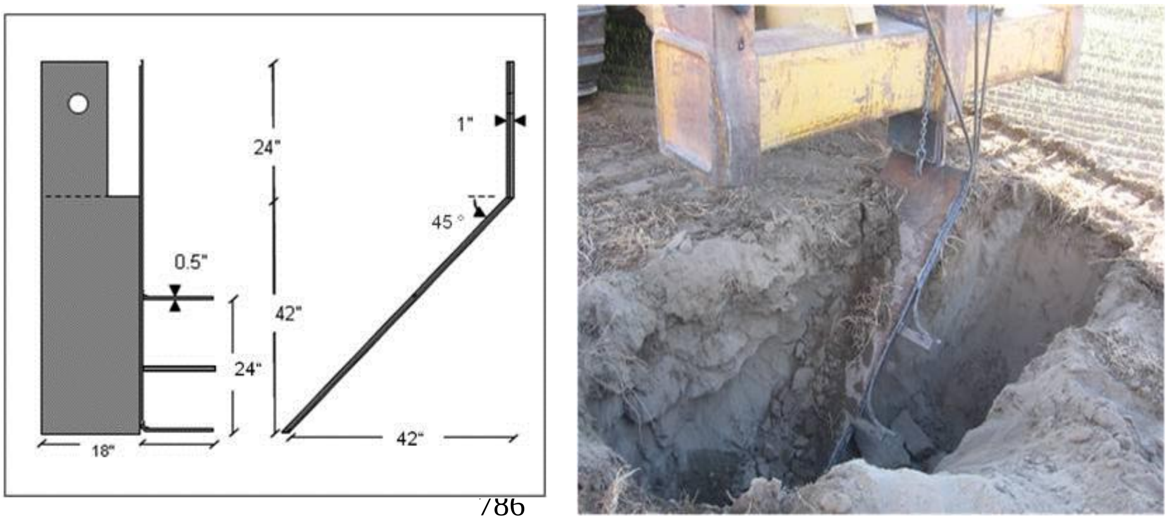

(a) (b)

Figure 2 (a) 45-degree "lift-plow" cable insertion tubes design (b) 45-degree "lift-plow" cable insertion tubes.

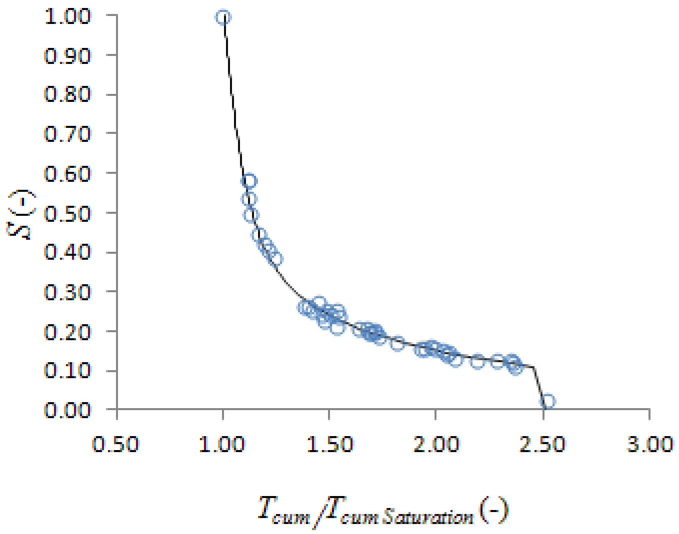

Figure 3 Calibration curve relating the degree of saturation (*S*) to T_{cum} normalized by its value at saturation integrated over 180 seconds for the 1–minute duration heat pulses. The calibration curve has the following form:

$$\boldsymbol{S} = \mathbf{0.0467} + (\mathbf{1.42} + \boldsymbol{T_{cum}/T_{cum\ Saturation}})/(\mathbf{-7.57} + \mathbf{10.1}\ \boldsymbol{T_{cum}/T_{cum\ Saturation}}{}^{\mathbf{2}}) \text{ for } S \geq 0.1$$

and

$$S = \mathbf{-0.5}\,\boldsymbol{T_{cum}/T_{cum\ Saturation}} + \mathbf{2.5}1 \text{ for } S < 0.1$$

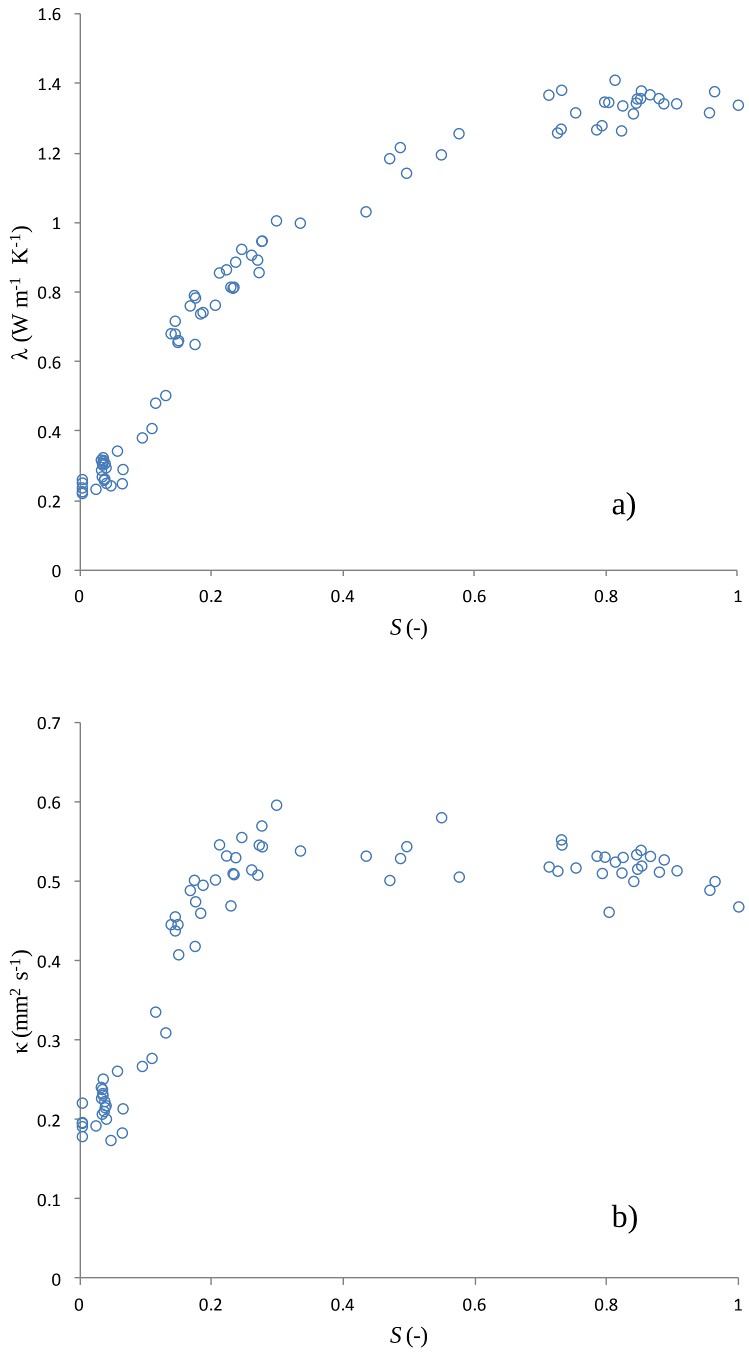

Figure 4 Degree of saturation (*S*) vs. a) thermal conductivity (λ) and b) thermal diffusivity (κ) measured from non-disturbed samples collected from the calibration soil column. After saturation, the samples were drained in a pressure chamber to allow measurement of λ at different level of soil water content using a KD2 Pro sensor.

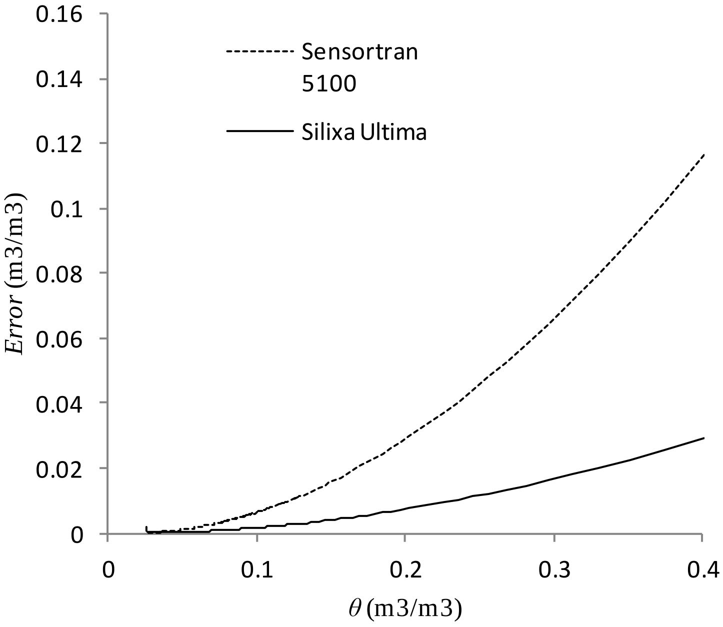

Figure 5 Estimated error in soil water content estimation due to the DTS system performance.

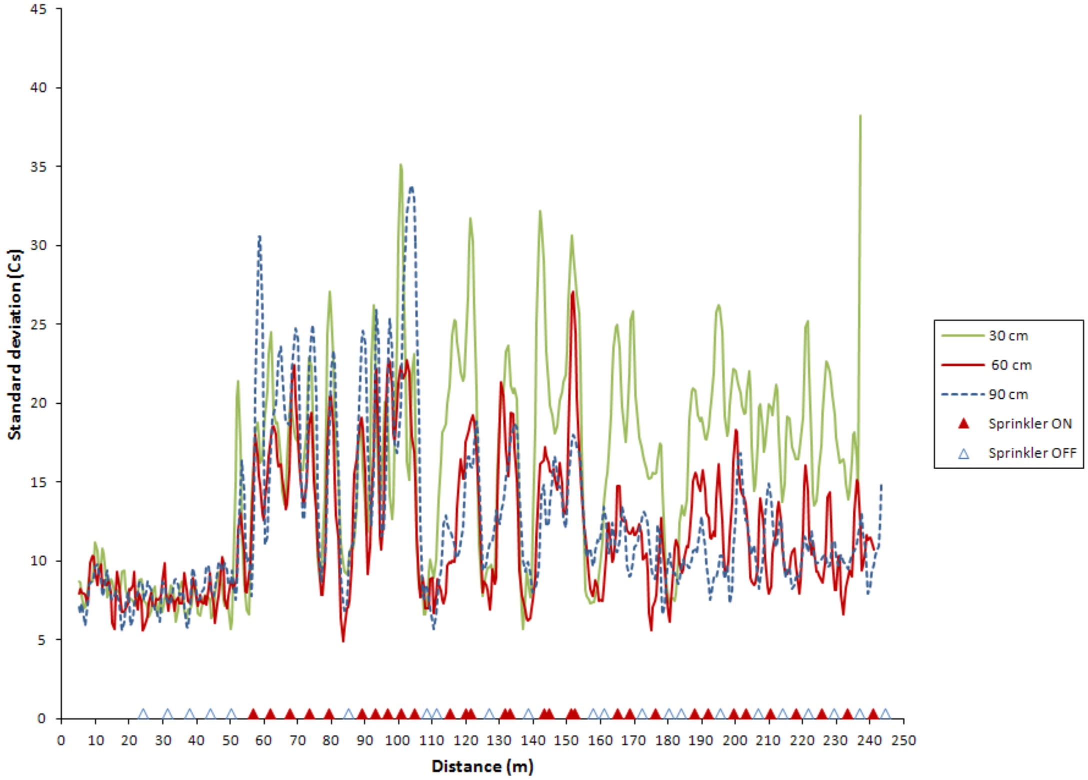

Figure 6 Observed standard deviation of T_{cum} at the 30, 60 and 90 cm depths during the 48 hr duration of the experiment.

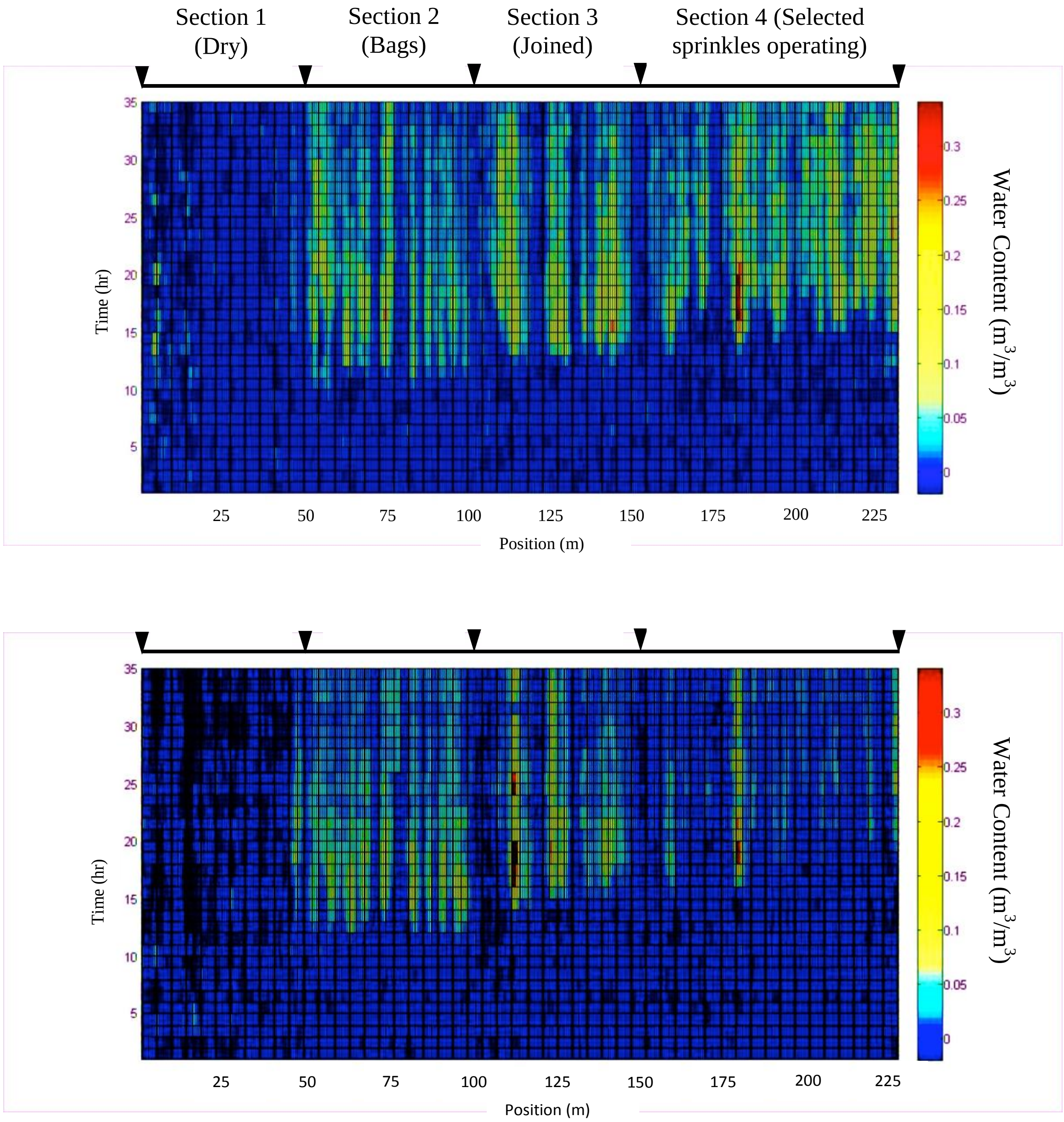

Figure 7 Soil water content change at the 30 cm (top figure) and 60 cm depths (bottom figure).

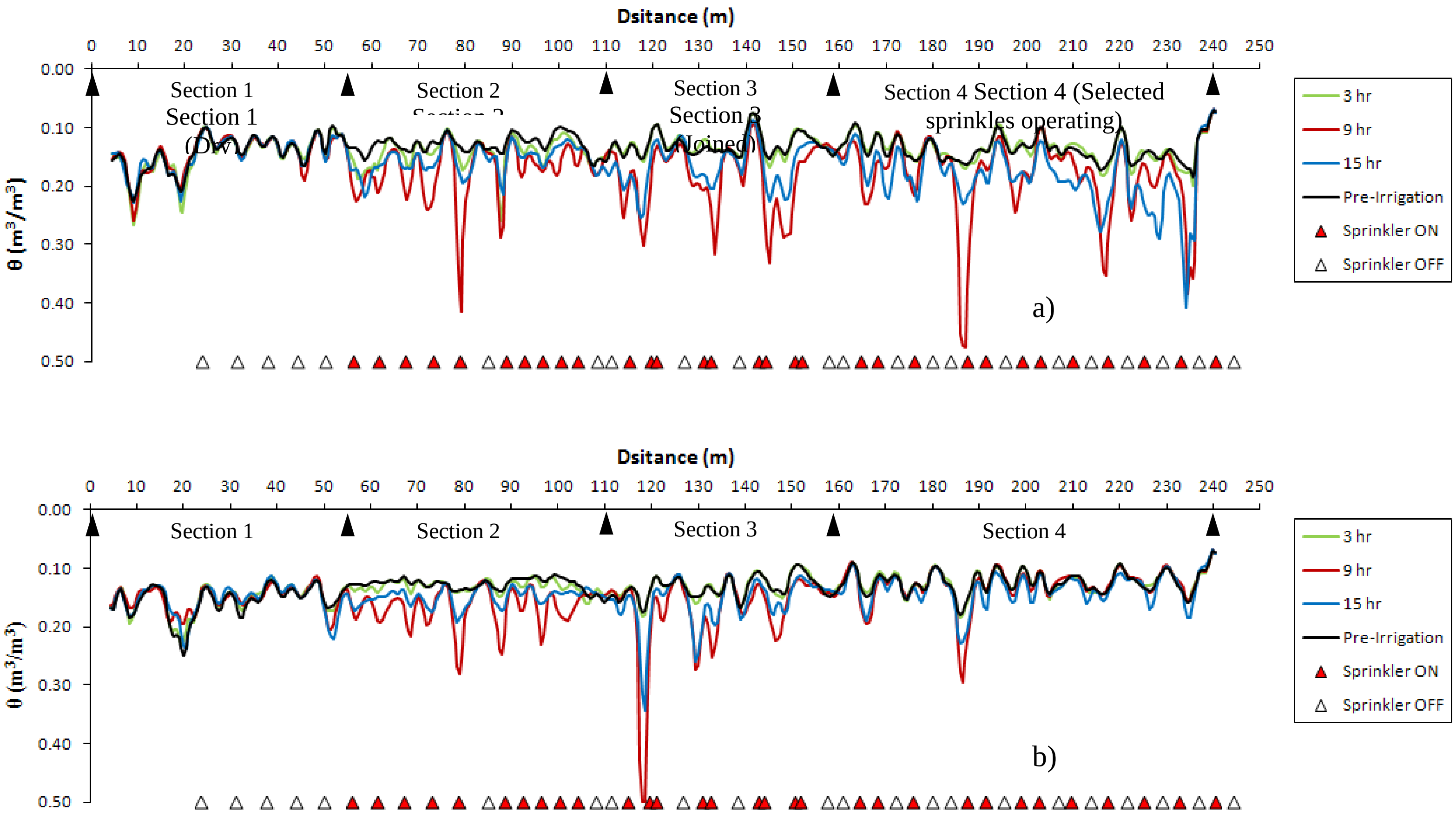

Figure 8 DTS estimated soil water content at a) 30 cm depth and b) 60 cm depth with emitter positions shown before , and at 3, 9, and 15 hours after the 7 hr irrigation set started.

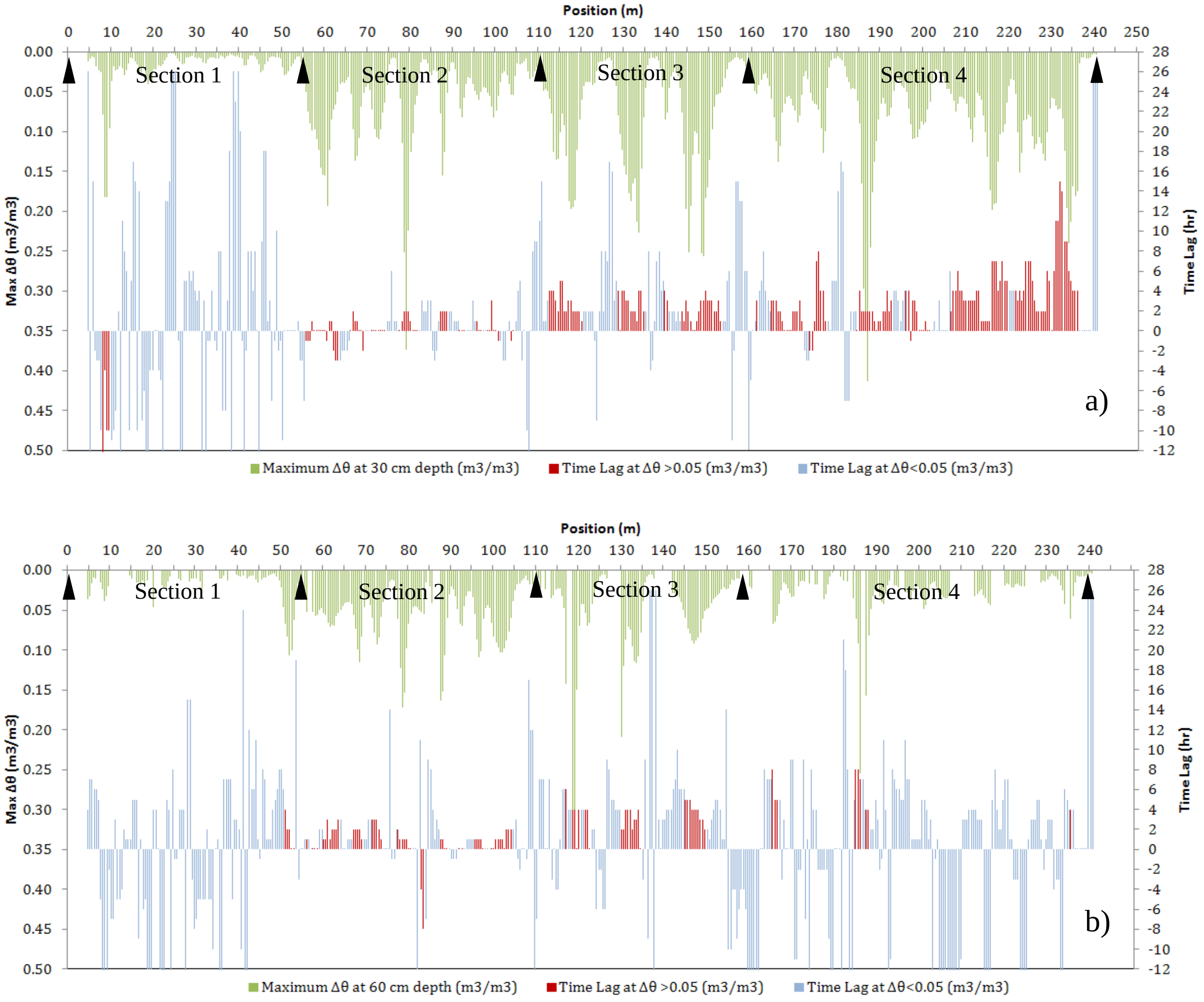
Position (m)
0
10
20
30
40
50
60
70
80
90
100
110
120
130
140
150
160
170
180
190
200
210
220
230
240
250
Max Δθ (m3/m3)
0.00
0.05
0.10
0.15
0.20
0.25
0.30
0.35
0.40
0.45
0.50
Time Lag (hr)
28
26
24
22
20
18
16
14
12
10
8
6
4
2
0
-2
-4
-6
-8
-10
-12
Section 1
Section 2
Section 3
Section 4
a)
Maximum Δθ at 30 cm depth (m3/m3)
Time Lag at Δθ >0.05 (m3/m3)
Time Lag at Δθ<0.05 (m3/m3)
Position (m)
Max Δθ (m3/m3)
Time Lag (hr)
Section 1
Section 2
Section 3
Section 4
b)
Maximum Δθ at 60 cm depth (m3/m3)
Time Lag at Δθ >0.05 (m3/m3)
Time Lag at Δθ<0.05 (m3/m3)

Figure 9 Time lag at the highest time-lagged correlation value a) between Δθ at 30cm and Δθ at 60 cm and b) between ΔT_{cum} at 60cm and ΔT_{cum} at 90 cm

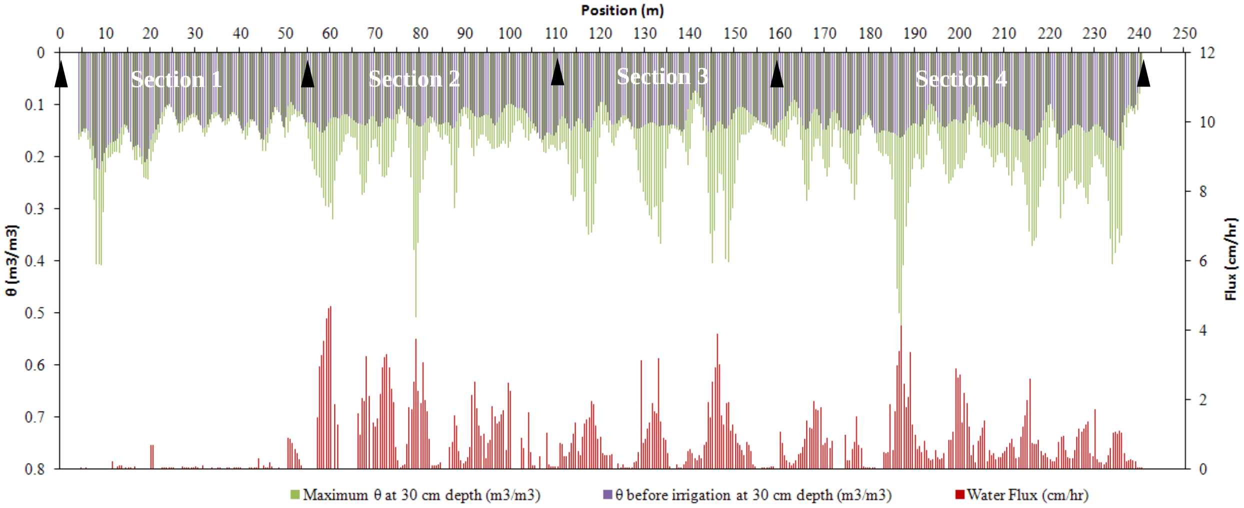
Position (m)
0
10
20
30
40
50
60
70
80
90
100
110
120
130
140
150
160
170
180
190
200
210
220
230
240
250
Section 1
Section 2
Section 3
Section 4
θ (m3/m3)
0
0.1
0.2
0.3
0.4
0.5
0.6
0.7
0.8
Flux (cm/hr)
12
10
8
6
4
2
0
🟩 Maximum θ at 30 cm depth (m3/m3)
🟪 θ before irrigation at 30 cm depth (m3/m3)
🟥 Water Flux (cm/hr)

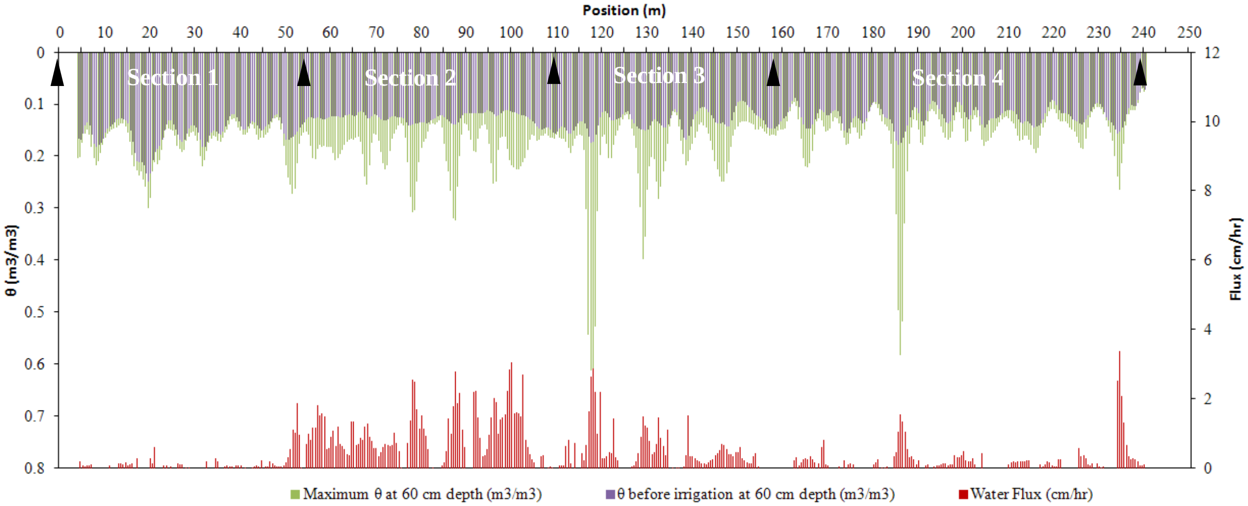
Position (m)
0
10
20
30
40
50
60
70
80
90
100
110
120
130
140
150
160
170
180
190
200
210
220
230
240
250
Section 1
Section 2
Section 3
Section 4
θ (m3/m3)
0
0.1
0.2
0.3
0.4
0.5
0.6
0.7
0.8
Flux (cm/hr)
12
10
8
6
4
2
0
🟩 Maximum θ at 60 cm depth (m3/m3)
🟪 θ before irrigation at 60 cm depth (m3/m3)
🟥 Water Flux (cm/hr)

Figure 10 Water flux, pre-irrigation soil water content, and maximum soil water content at the 30 cm depth (top figure), and at the 60 cm depth (bottom figure)

Table 1 Soil physical and hydraulic properties (USDA Natural Resources Conservation Service, 2006).

Depth (cm)	Bulk density (g cm^{-3})	Sat. Hydr. Conductivity m s^{-1}	Available Water capacity (cm^3 cm^{-3})	Organic matter (%)
0-10	1.15-1.30	14.4-50.4 10^{-6}	0.14-0.17	0.7-1.0
10-89	1.20-1.50	14.4-50.4 10^{-6}	0.14-0.17	0.0-1.0
89-152	1.40-1.70	14.4-50.4 10^{-6}	0.14-0.17	0.0-1.0

Table 2 Lower bounds on averages fluxes (cm h^{-1}), by section, at 30 and 60 cm depths.

	Section 3			**Section 4**		
	$\Delta\theta \geq 0.5$ m^3 m^{-3}	$\Delta\theta < 0.5$ m^3 m^{-3}	All locations	$\Delta\theta \geq 0.5$ m^3 m^{-3}	$\Delta\theta < 0.5$ m^3 m^{-3}	All locations
Average Flux at 30 cm depth (cm h^{-1})	>1.3	>0.2	>0.8	>0.9	>0.2	>0.8
Average Flux at 60cm depth (cm h^{-1})	>1.1	>0.3	>0.5	>1.0	>0.1	>0.2
Average Flux applied at the surface (cm h^{-1})	-	-	1.0	-	-	0.8